



Optics Letters

Micro-sized tunable liquid crystal optical filters

CALEB STOLTZFUS,¹ RUSSELL BARBOUR,² DAVID ATHERTON,¹ AND ZEB BARBER^{1,*}

¹Spectrum Lab, Montana State University, Bozeman, Montana 59717, USA

²Advanced Microcavity Sensors, Bozeman, Montana 59715, USA

*Corresponding author: zeb.barber@montana.edu

Received 14 March 2017; revised 26 April 2017; accepted 30 April 2017; posted 3 May 2017 (Doc. ID 290665); published 22 May 2017

Liquid crystal arrayed microcavities (LCAM) is a new technology for ultra-narrow optical filtering (FWHM ~ 0.1 nm) that uses picoliter volume Fabry–Perot-type optical cavities filled with liquid crystal for tuning. LCAMs are sub-nm spectral resolution filters, which utilize well-established laser writing, thin film deposition, and wafer manufacturing techniques. These filters are compact, robust, and inexpensive. Compact, high-resolution optical filters have applications, including biomedical imaging, chemical detection, and environmental monitoring. Here, we describe the LCAM design and initial performance metrics. ©2017 Optical Society of America

OCIS codes: (230.0230) Optical devices; (230.3720) Liquid-crystal devices; (230.3990) Micro-optical devices; (230.7408) Wavelength filtering devices; (160.3710) Liquid crystals; (120.2230) Fabry-Perot.

<https://doi.org/10.1364/OL.42.002090>

Tunable optical filters come in many shapes, sizes, and complexities, each addressing the unique requirements of disparate applications that need various bandwidths, tuning speeds, and spectral tuning ranges. Piezoelectrically driven, air-gap Fabry–Perot filters [1–6], microcavity filters [7–11], birefringent filters [12–14], and liquid-crystal (LC)-based devices [15–19] have been used to fill the various requirements of different applications.

LC tunable filters (LCTFs) have been used for Raman imaging, chemical detection, hyperspectral imaging, and many other applications [5,17–21]. LCTFs are typically either Fabry–Perot or Lyot-type filters. The use of LC to tune the peak transmission wavelength allows for robust, non-mechanical, low voltage controlled tunable filtering of input light. Commercially available LCTFs cover a broad range of wavelengths. However, they typically have limited spectral resolution (limited by the achievable parallelism of the mirrors and no lateral confinement) and can be relatively large in size. These filters have a FWHM > 5 nm tunable bandpass and transmission window and exhibit maximum transmission, $T = 5\% - 60\%$, for polarized light.

Lyot-type filters use multiple birefringent plates sandwiched between parallel polarizers to achieve spectral selection [13,17]. Using LC in the birefringent plates allows for electrical tuning of the transmission wavelength. Lyot-type filters typically have

high attenuation due to the use of stacked polarizers [13]. These filters have a broad acceptance angle, requiring no mode coupling, which makes them ideally suited for many applications.

Fabry–Perot-type microcavity filters constructed from two closely spaced mirrors (spaced with an air-gap < 2 μm) are also used to filter broadband light. Recent advances in microcavity technology have been primarily driven by the need for high finesse and small mode volume cavities in the field of atomic physics and solid-state cavity QED [6]. Several groups have constructed open-access optical microcavities formed by a microscopic curved mirror and a planar mirror combination that demonstrates a cavity finesse that is limited only by the quality of the mirror coatings [1,3–5]. A cavity finesse of more than 100,000 has been demonstrated [22]. The distance between the mirrors determines the transmission wavelength, which is tuned using piezoelectric actuators. These filters provide very narrow transmission bandwidths, $\Delta\lambda \ll 1$ nm. The use of piezos to tune the air-gap length introduces challenges for a useful commercial device such as drift, hysteresis, and non-linearity. When used in mechanically isolated and thermally controlled cryogenic environments, the majority of piezo issues are resolved and these filters have demonstrated excellent performance [4].

Many applications require a robust, room temperature, sub-nm resolution, and a continuously tunable filter. By combining liquid LC tuning with Fabry–Perot-type microcavities, the filters described here achieve all of these specifications [23]. Our current design, using mirrors with a peak reflectivity of 99.4%, provides continuously tunable transmission that is less than 0.3 nm FWHM over a 200 nm (550–750 nm) bandwidth and with a free spectral range (FSR) of 20–70 nm. With higher reflectivity mirrors, transmission widths of tens of picometers can be achieved. A 10–100 μm diameter curved coupling mirror on one of the Fabry–Perot mirror surfaces forms a stable picoliter-sized optical cavity. A voltage across the LC between the two mirrors tunes the index of refraction of the LC, which tunes the peak transmission wavelength of the filter for linearly polarized light, whose polarization is aligned with the LC molecules, while the peak transmission for orthogonally polarized light remains fixed. This means the tunable transmission is only effective for one polarization, and external polarization optics are required to filter out or address the orthogonal polarization. The use of a monolithic, fixed-gap design reduces the

susceptibility of the filter to noise from vibrations and temperature changes.

In this Letter, we discuss the development and characterization of our LC arrayed microcavities (LCAM). An LCAM consists of a two-dimensional (2D) array of many narrowband tunable microcavity filters. Each cavity can be used as a single element or combined into an interconnected spatial array. These filters enable highly miniaturized spatial/spectrally resolving devices for material characterization, biomedical imaging, hyperspectral microscopy, and other applications.

Figure 1(A) shows the basic schematic of a single microcavity channel of an LCAM. A miniature (10–100 μm) diameter depression is laser written into a fused silica substrate. A conductive indium tin oxide (ITO) and a high reflection (>99%) multi-layer dielectric mirror coating at the desired wavelength is deposited on top of this substrate. A stable Fabry–Perot cavity is formed with a second flat mirror with the same ITO and mirror coating. The mirrors are spaced by a thin ($L > 1 \mu\text{m}$) gap, which is filled with a nematic LC oriented with a very thin (<100 nm) alignment layer. The ITO layers allow low voltage control of the LC tuning layer. Figure 1(B) shows a completed LCAM filter coupled to a fiber with bulk coupling optics. A large array of these channels could be integrated with complementary metal-oxide-semiconductor (CMOS) or CCD detectors to rapidly collect both spatial and spectral information from an illuminated object or biological sample.

A flow chart of the fabrication process is shown in Fig. 2. We start by ablating shallow arrays of craters onto 4 in fused silica wafers (University Wafer Part #: U01-131126-11 JGS2, $R_a < 1 \text{ nm}$). The ablation process melts the fused silica, and surface tension makes the surface of the curved mirror atomically smooth. The depth of the craters was varied from

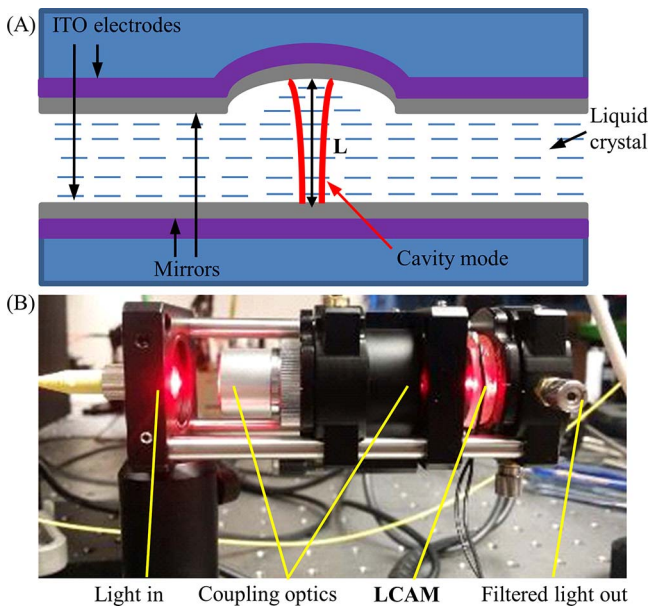


Fig. 1. (A) LCAM schematic showing a conceptual design of a single optical microcavity (not to scale). The cavity medium contains a homogeneous planar aligned nematic LC layer (blue dashes), allowing the effective cavity length to be tuned. (B) Current device undergoing benchtop testing. The monolithic compact package is low cost, highly ruggedized, and operates well at room temperatures.

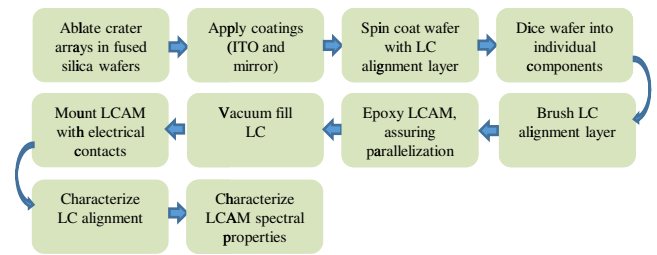


Fig. 2. Flowchart of the LCAM manufacturing steps.

0.2 μm up to 6 μm , with a corresponding radius of curvature of 1300 μm down to 50 μm . The craters are ablated using the 10.6 μm line of a tightly focused CO_2 laser (Synrad, FSV30SFG). The CO_2 laser is focused onto the wafer using a ZnSe lens ($f = 15 \text{ mm}$). The intensity of the white light emitted by the plasma generated in the ablation process is used in a feedback circuit to control the laser energy absorbed by the substrate, which is proportional to the depth of the crater. The laser ablation for a single crater occurs in less than 50 μs . Arrays of craters are ablated using an automated LabVIEW program, where computer controlled stages (Zaber, T-LS28E) move the wafer to the position of each crater. Ablating a 10×10 array of 220 μm spaced craters takes only a couple minutes, limited mostly by the motion of the stages, which could be greatly improved. Many such arrays can be written on a single wafer. Half of the wafer area, or separate wafers, are reserved (no ablated craters) to form the flat portion of the microcavities.

Once multiple arrays of craters have been ablated, all of the wafers were coated by Optical Filters Source, LLC in Pflugerville, Texas. First a 180 nm thick layer of ITO is deposited. The conductive ITO layer allows for voltage control of the LC. In some cases, the ITO layer is patterned to allow simultaneously addressing craters from the same array with different voltages. Placing the optically lossy ITO layer underneath the high reflectivity mirror eliminates this as a source of optical loss in the Fabry–Perot cavity and only slightly increases the required tuning voltage. After the ITO has been deposited, seven pairs of $\text{TiO}_2/\text{SiO}_2$ mirror coatings are deposited, yielding a peak reflectivity of 99.4% centered at 615 nm. The high reflectivity mirror coating determines many of the properties of the final LCAM device, including wavelength coverage and resolution of the Fabry–Perot resonances. Broadband dielectric mirror designs can be used to increase the wavelength coverage, but require more layers, which can increase the losses due to the mirrors and affect the filter tuning due to the dispersion characteristics of the coating.

Once the ITO and mirror coatings have been deposited, the wafers without craters are spin coated with a $\sim 100 \text{ nm}$ thick layer of 2% polyvinyl alcohol (PVA) dissolved in deionized (DI) water, which forms the LC alignment layer. After this, the wafers with craters are diced into 9.5 mm \times 9.5 mm square pieces, and the wafers without craters are diced into 12.7 mm \times 12.7 mm square pieces. The difference in size between the two mirror pieces allows for easy access to the conductive ITO layer after the LCAM assembly.

To align the LC, we gently drag lens tissue across the PVA layer hundreds of times. Once the alignment layer has been brushed, we fix the two mirror surfaces together using UV cure epoxy (Norland UV sealant 91 epoxy) mixed with $\sim 1 \mu\text{m}$

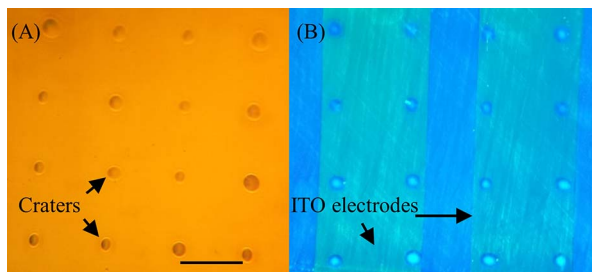


Fig. 3. (A) Reflected light microscope image of the craters in an LCAM. (B) Polarization microscope image showing excellent LC alignment over an array of LCAM channels. The PVA alignment layer was fabricated as described in the text. The greenish strips are ITO electrodes that enable independent tuning of different LCAM channels, and the circles are the craters in the mirror surface. The scale bar is 200 μm .

diameter silica spacer beads (Cospheric, SiO₂MS-1.8 0.961 μm). Before the epoxy is cured, a custom jig is used to assure that the mirror pieces are parallel by centering the Newton rings. Typically, this method yields a sufficiently parallel gap over the small area of an individual optical cavity. To fill the gap between the mirrors with LC, the LCAM unit is placed in a vacuum chamber, and a drop of LC is placed on the edge of the LCAM, where it can drain into the gap. After the LC is placed on the LCAM, the vacuum pump is turned on as soon as possible. The vacuum chamber pumps down to a modest vacuum much faster than the LC fills the cavity, which ensures that air bubbles are minimized in the final LC fill. For the LCAMs described here, either 5CB or E7 LCs were used. The LC alignment and LC filling is checked with a polarization microscope. Microscope images of the craters and LC layer are shown in Fig. 3. For some LCAMs, the unit is

heated to beyond the clearing temperature of the LC for a few minutes to achieve good LC alignment.

Figures 4(A) and 4(B) show the characteristic transmission of a single LCAM optical cavity with broad white LED light illumination. Figure 4(C) shows the characteristic transmission of the same optical cavity with 632 nm HeNe laser illumination. In both cases, the illumination was coupled to a single optical cavity using a 40 \times , 0.45 NA microscope objective. A 60 kHz square wave with a varying peak-to-peak voltage (V_{pp}) is applied to the ITO layers to control the orientation of the LC molecules. As the voltage across the LC is varied from 0 to 10 volts, the peak transmission tunes to shorter wavelengths. Each horizontal row in Fig. 4(A) represents a full spectrum of the LCAM transmission, corresponding to each LC voltage. The transmission spectrum when $V_{pp} = 2.54$ V is shown in Fig. 4(B). The reflectivity of the mirror coatings, although not perfectly spectrally flat, is at least greater than 90% within the wavelength region between 550 and 750 nm, allowing the transmission to be tuned anywhere within this 200 nm wavelength range. This range can be set by changing the mirror coatings. The FSR and the FWHM of the transmission peaks can be adjusted by changing the spacing between the mirrors. As can be seen in the bottom portion of Fig. 4(A), below $\sim 1V_{pp}$, the LC does not respond and no tuning occurs. Above the $1V_{pp}$ threshold, the transmission of each peak can be tuned across 67 nm.

Figure 5 shows the performance of multiple optical cavities from different LCAM units. The finesse refers to the ratio of the FSR divided by the bandwidth (FWHM) of a single transmission peak. Finesse is independent of the FSR of the cavity and is a measure of the optical scattering losses in the cavity. The 632 nm line of a HeNe laser was used to measure the FWHM. The laser was coupled to a microcavity, and the transmission was measured as a function of V_{pp} . Wavelength versus V_{pp} data, as is shown for a single cavity in Fig. 4(A), was used to

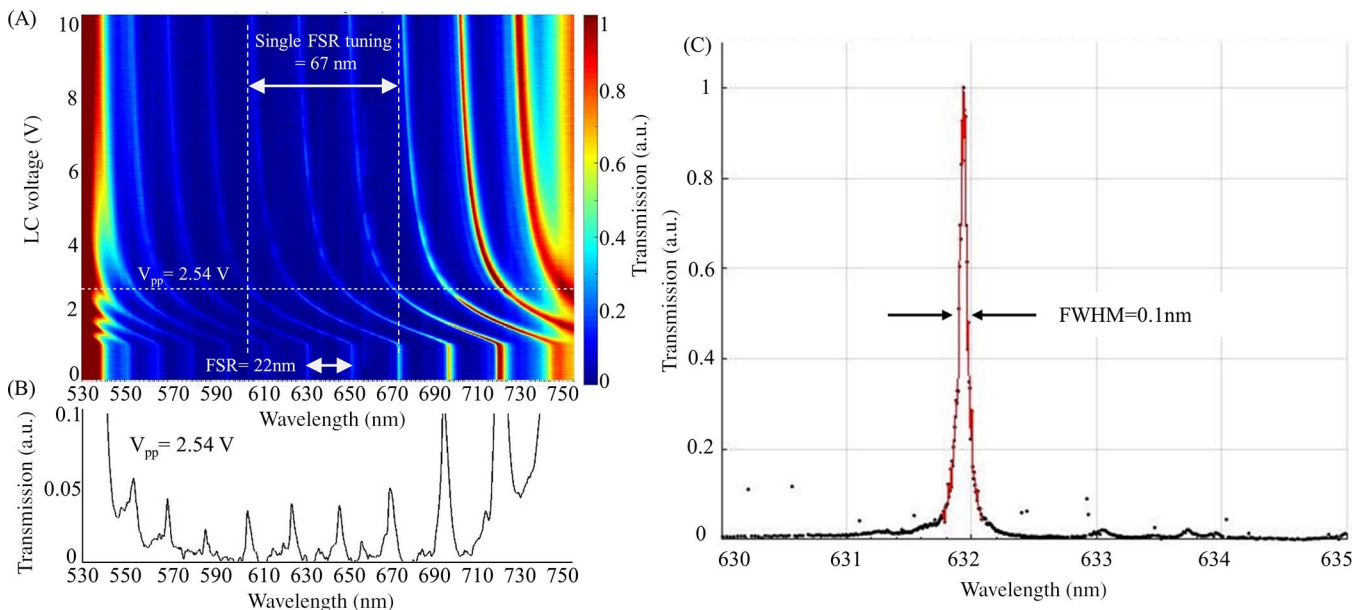


Fig. 4. (A) Transmission of a single LCAM cavity, from LCAM 3, with spectrally broad illumination. Cavities are tunable over a wide wavelength range. (B) Spectrum of the LCAM transmission corresponding to $V_{pp} = 2.54$ V. The limited resolution of the spectrometer (2 nm resolution, Stellarnet, GREEN-Wave) makes the transmission peaks appear broader and dimmer than they should. (C) Transmission of the same LCAM channel with 632 nm HeNe illumination, recorded with high spectral resolution.

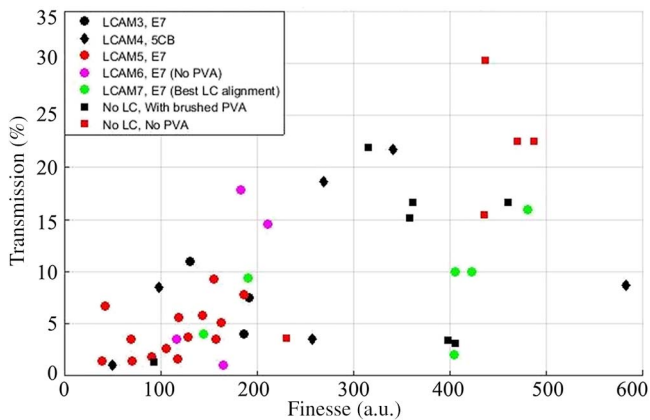


Fig. 5. Transmission versus finesse plot for a selection of optical cavities from different LCAM units.

calibrate the conversion from V_{pp} to wavelength. In Fig. 4, small transverse mode transmission peaks can be observed. These are suppressed with good alignment to the TEM00 mode of the optical cavity. In applications where good alignment cannot be achieved, deconvolution of the characterized transmitted spectrum may be required.

Each LCAM unit has 100 optical cavities in a 10×10 array. Multiple units were made with either E7, 5CB, or no LC. The uniformity of the LC alignment layer varied when different brushing techniques were used. The most successful technique involved lightly brushing the PVA layer with lens cleaning tissue hundreds of times, as previously described. This technique was used for all LCAMs described here. The two LCAM units with no LC used piezoelectric mounts to scan the physical distance between the mirrors.

The data shown in Fig. 5 suggest that the LC could somewhat reduce the quality of the resonator. However, it appears that as more LCAMs were assembled, their properties improved, with some achieving near the theoretical finesse of 522 limited by the 99.4% reflectivity of the cavity mirrors. This is likely due to the fact that the final steps of assembling the LCAM units is done by hand and takes some skill, which improved with practice. There is significant variation of both the finesse and the transmission from cavity to cavity. The most likely cause of this is particulate matter left in the craters from the ablation process, handling in non-cleanroom environments, and local defects in the dielectric mirror and PVA coatings. Some craters appeared to have very little contamination and defects and some had lots. Improvements to the ablation and manufacturing processes should yield more uniform cavity performance.

In summary, the development and characterization of initial LCAMs yielded sub-nm resolution, room temperature, tunable filters. Future improvements to the LCAM design will increase the operation range for a wider accessible wavelength region and increased uniformity of individual cavities across arrays. We aim to expand LCAM spectral coverage to the near

infra-red (NIR) during the next phase of development. The long-term vision for the LCAM technology is a low-cost, integrated, and versatile hyperspectral/ultra-spectral imager, which will have high spectral resolution, a low cost-to-performance ratio, and be ultra-compact. These miniaturized filters enable devices for material characterization, biomedical imaging, hyperspectral microscopy, and other applications.

Funding. National Science Foundation (NSF) (1548568); Montana Board of Research and Commercialization Technology (16-50-001); U.S. Air Force (USAF) (FA8650-15-M6656 PHASE I, FA8650-16-C-6723 PHASE II).

Acknowledgment. The authors thank Dr. Daniel Farkas and Dr. Nicholas Booth of Spectral Molecular Imaging, Inc., and Dr. Krishna Rupavatharam for many useful conversations. We also thank Frank Calcagni from Optical Filter Source Inc., Tom Baur from Meadowlark Optics, and Dr. Hiroshi Yokoyama from Kent State University for useful advice on fabrication and liquid crystal alignment.

REFERENCES

1. R. J. Barbour, P. A. Dalgarno, A. Curran, K. M. Nowak, H. J. Baker, D. R. Hall, N. G. Stoltz, P. M. Petroff, and R. J. Warburton, *J. Appl. Phys.* **110**, 053107 (2011).
2. D. Hunger, C. Deutsch, R. J. Barbour, R. J. Warburton, and J. Reichel, *AIP Adv.* **2**, 012119 (2012).
3. D. Hunger, T. Steinmetz, Y. Colombe, C. Deutsch, T. W. Hänsch, and J. Reichel, *New J. Phys.* **12**, 065038 (2010).
4. L. Greuter, S. Starosielec, D. Najer, A. Ludwig, L. Duempelmann, D. Rohner, and R. J. Warburton, *Appl. Phys. Lett.* **105**, 121105 (2014).
5. M. Kuznetsov, M. Stern, and J. Coppeta, *Opt. Express* **13**, 171 (2005).
6. K. J. Vahala, *Nature* **424**, 839 (2003).
7. A. Poon, F. Courvoisier, and R. Chang, *Opt. Lett.* **26**, 632 (2001).
8. Z. Di, H. V. Jones, P. R. Dolan, S. M. Fairclough, M. B. Wincott, J. Fill, G. M. Hughes, and J. M. Smith, *New J. Phys.* **14**, 103048 (2012).
9. G. Ctistis, A. Hartsuiker, E. van der Pol, J. Claudon, W. L. Vos, and J.-M. Gérard, *Phys. Rev. B* **82**, 195330 (2010).
10. C. Reese, C. Becher, A. Imamoğlu, E. Hu, B. D. Gerardot, and P. M. Petroff, *Appl. Phys. Lett.* **78**, 2279 (2001).
11. P. R. Dolan, G. M. Hughes, F. Grazioso, B. R. Patton, and J. M. Smith, *Opt. Lett.* **35**, 3556 (2010).
12. J. Evans, *J. Opt. Soc. Am.* **48**, 142 (1958).
13. O. Aharon and I. Abdulhalim, *Opt. Express* **17**, 11426 (2009).
14. G. Shabtay, E. Eidinger, Z. Zalevsky, D. Mendlovic, and E. Marom, *Opt. Express* **10**, 1534 (2002).
15. S. Isaacs, F. Placido, and I. Abdulhalim, *Appl. Opt.* **53**, H91 (2014).
16. J. S. Patel, M. A. Saifi, D. W. Berreman, C. Lin, N. Andreadakis, and S. D. Lee, *Appl. Phys. Lett.* **57**, 1718 (1990).
17. H. R. Morris, C. C. Hoyt, P. Miller, and P. J. Treado, *Appl. Spectrosc.* **50**, 805 (1996).
18. M. Abuleil and I. Abdulhalim, *Opt. Lett.* **41**, 1957 (2016).
19. I. August, Y. Oiknine, M. AbuLeil, I. Abdulhalim, and A. Stern, *Sci. Rep.* **6**, 23524 (2016).
20. D. L. Farkas and D. Becker, *Pigment Cell Res.* **14**, 2 (2001).
21. A. O. H. Gerstner, W. Laffers, F. Bootz, D. L. Farkas, R. Martin, J. Bendix, and B. Thies, *J. Biophoton.* **5**, 255 (2012).
22. C. J. Hood, H. J. Kimble, and J. Ye, *Phys. Rev. A* **64**, 033804 (2001).
23. R. Barbour and Z. Barber, "Microcavity array for spectral imaging," WO patent application WO2016057125A1 (April 14, 2016).